A CALCULATIONAL ROUND ROBIN IN ELASTIC-PLASTIC FRACTURE MECHANICS

L.H. Larsson

Commission of the European Communities
Joint Research Centre, Ispra Establishment
Applied Mechanics Division
21020 Ispra - Italy

Extended version of a paper presented at the 6th Int. Conference on Structural Mechanics in Reactor Technology, Paris, 17-21 August 1981, Paper G 3/2.

Submitted for publication in the Int. Journal of Pressure Vessels and Piping.

ABSTRACT

Eighteen organizations participated in this round robin which treated the same three-point bend problem as an ASTM round robin four years earlier. Overall deformation, J, CTOD and crack profile were the main results required using plane strain elastic-plastic finite element analysis for a monotonically increasing load up to a maximum deformation which was far beyond the elastic regime.

All elastic solutions were accurate to within a few percent. In the elastic-plastic regime, however, there was a large scatter of the results, increasing with increasing plastic deformation and roughly of the same order as in the ASTM round robin which contained ten solutions. Apparently no significant progress has taken place in the state of the art of numerical EPFM analysis in four years time. The paper discusses the reasons for this scatter and draws tentative conclusions on the most suitable numerical analysis methods in EPFM.

1. INTRODUCTION

Elastic-plastic fracture mechanics (EPFM) is receiving an important research effort all over the world in order to address fracture problems in cases where linear elastic fracture mechanics (LEFM) is not applicable. Experimental work has shown that the J-integral [1] and the crack tip opening displacement (CTOD) are promising parameters for characterising crack behaviour in tough materials. For monotonically increasing loading the latter includes crack tip blunting followed above the initiation point by slow stable crack growth up to the point of tearing instability.

The reliability of safety assessments of cracked elastic-plastic bodies is dependent on (1) the reliability of experimental methods for measuring J and CTOD, (2) the reliability of the criteria which use J, CTOD or parameters derived from them for describing crack behaviour and, (3) the reliability of numerical methods for predicting these parameters. The first point is concerned with standardizing specimens and measurement methods. The second point involves comparisons between numerical predictions and experiments and requires also validations on structural members. This paper adresses the third aspect.

It would seem tempting to require that numerical methods should be able to predict J and CTOD with at least the accuracy by which critical values of these parameters can be measured. In the absence of analytical solutions of elastic-plastic crack problems, it is not easy to evaluate the accuracy of numerical solutions. A round robin offers an attractive possibility in this respect. When the same problem is solved by a large number of persons independently, using various computer codes and choosing freely the type of discretization, the

scatter of the results gives a measure of the accuracy that one can expect from such calculations. Furthermore, from a comparison of the solutions one can try to draw conclusions on the most suitable methods for treating elastic-plastic problems.

The Joint Research Centre (JRC), Ispra Establishment of the Commission of the European Communities, has included the organization of numerical EPFM round robins in its Reactor Safety Research Program. In 1979, the problem specifications of a first numerical round robin were defined in collaboration with the Task Group on EPFM (Chairman Dr. J.D. HARRISON, Welding Institute, UK) of the European Group on Fracture. Table 1 gives the list of the eighteen organizations which participated in the present round robin and the names of the correspondents. They represent nine European countries and the JRC itself.

2. DESCRIPTION OF THE PROBLEM

The problem considered in this round robin is the same as that treated by ASTM Committee E24 Task Group E24.01.09 in 1976 [2].

Fig. 1 shows the geometry and loading conditions which represent a three-point bend specimen. Fig. 2 shows the imposed uniaxial true stress-strain curve. The latter has been subdivided into a linear portion and a power law portion contrarily to [2] in which no linear part existed; however, the difference between the corresponding curves is negligible. The material Poisson ratio is $\nu = 0.3$.

It is sufficient to analyze the upper half of the specimen due to symmetry. The horizontal displacement of point C is fixed ($u_C = 0$), therefore the load-point deflection is given by the u-displacement of point A, u_A.

Required plane strain analysis results include the following:

a) Elastic solution

Dimensionless stress intensity factor $K_1 \, W^{\frac{1}{2}} \, B/P$

Dimensionless load-point compliance $u_A \, EB/P$

Dimensionless crack mouth opening displacement $2 v_B \, EB/P$

K_1 is to be calculated from

$$K_1 = \left[E\bar{J}/(1-\nu^2) \right]^{\frac{1}{2}} \qquad (1)$$

where $\bar{J}$ is a mean value of J integrals calculated over several paths enclosing the crack tip (i.e. the value of J judged to be the most representative by each investigator).

b) Elastic-plastic solution

Variation of deflection, J and CTOD for a monotonically increasing load up to the point where $u_A = 1.5$mm. This is far in the elastic-plastic regime since the elastic part of the displacement is then about one quarter of the total displacement. J is again taken as the mean value around a number of paths, $\bar{J}$. The specified procedure for calculating CTOD consists in taking the distance between the points at which a + 45 degree line and a -45 degree line drawn from the actual crack tip intersect the crack profile. The crack profile along the first 10 per cent of the ligament,

starting from the crack tip, is to be plotted. Furthermore, due to the interest in the usual experimental procedure for determining J, it is requested to calculate J also from the load-deflection curve:

$$J_u = \frac{2}{B(W-a)} \int_0^{u_A} P du_A \qquad (2)$$

3. COMPUTER CODES AND MODELLING

All eighteen participants used finite element codes based on the displacement formulation. Table 2 lists these codes and the options which were applied to the present problem. Without exception these codes apply the flow theory (incremental theory) of plasticity and the Von MISES yield criterion with the normality rule for plastic flow. Isotropic hardening was used in all solutions except in No. 2 which adopted the Besseling fraction model; this was tantamount to applying a combination of isotropic and kinematic hardening.

As required, plane strain analysis was applied in all solutions, except in No. 1 where generalized plane strain was imposed. The resulting spatially constant strain in the z – direction was, however, relatively small, never exceeding 3×10^{-5}.

Some participants reported more than one solution, thus the total number of available solutions is well over twenty. However, only one solution per participant is reported here, namely the one considered by the participant himself to be the most accurate. Occasionally some indications on the other solutions will be given.

Two of the eighteen solutions (Nos. 5 and 15) were obtained from a large strain/displacement analysis. Solution No. 5 accounted for finite geometry changes by the updating of nodal coordinates and by applying appropriate rotations to the accumulated inelastic strain tensor. Solution No. 15 used the total Lagrange formulation of the ADINA code. Rather than trying to give an exhaustive description of the applied numerical methods, Table 2 is intended to convey an idea

of the wide variety of methods and options used in the different solutions. For instance, equilibrium iterations within each load increment were applied in most solutions. Here, those solutions in which the load unbalance vector is calculated once per load step and added to the load increment of the next step are reported as having no equilibrium iteration.

The number of loading steps varied from 12 to 564. One half of the solutions imposed load increments, the other half displacement increments. Amongst the cases with the smallest number of loading steps, solutions 11,12 and 17 applied 15 equal displacement increments of 0.1mm, solution 16 12 variable load increments decreasing with increasing deformation. The latter solution stopped at u_A=1.1mm. The author of solution 14 reported he had also made the analysis with 20 loading steps instead of 60 and obtained practically the same results.

The last column in Table 2 shows how the given uniaxial stress-strain curve was approximated. Indeed, although in the majority of the solutions the specified stress-strain curve was implemented exactly, various approximations were introduced in other solutions. These approximations can be considered to be very close to the exact curve except in solutions 3 and 5 where some deviations appear in the vicinity of the initial yield stress and in solution 8 which adopted a bilinear approximation.

Table 3 shows the main features of the finite element discretization in the elastic-plastic field; in some cases the FE models used in the elastic field were slightly different. Solutions 1-3 and 18 use constant strain triangles, solutions 4-6 4-node quadrila-

terals and solutions 7-17 8-node quadrilaterals. The number of degrees of freedom varied from 236 in solution 18 to 952 in solution 4, most frequently it was in the range 400-700. Crack tip elements designated by normal elements in Table 2 refer to the same elements as in the far field. Their size ranged from 0.08 to 0.5mm in the models using constant strain triangles, from 0.13 to 0.635mm for the 4-node quadrilaterals and from 0.25 to 2.2mm for the models containing 8-node isoparametric elements. In the latter case, crack tip elements were either normal isoparametric triangles or quadrilaterals, or quadrilaterals collapsed into triangles.

4. COMPARISON OF THE RESULTS

4.1 Elastic solutions

Table 4 gives the non-dimensional results of the elastic analysis and some details on the J calculations. The data reported for the J calculations concern those paths which were effectively used for calculating $\bar{J}$. In several cases a number of other paths were used but they were rejected due to the resulting larger scatter. Furthermore, some participants made additional J calculations using the virtual crack extension method or other methods. For consistency, only the path integral results are reported here except for solution 14. $\bar{J}$ was always calculated as the arithmetic mean of the reported number of J values. The mean radius of the integration path is the radius of a circle having the area enclosed by the integration path.

As can be seen from Table 4, the scatter of the J values along the different paths was small, never exceeding $\pm$ 5% of $\bar{J}$ but often

remaining within $\pm$ 1%. The dimensionless stress intensity factor $K_1 W^{\frac{1}{2}} B/P$ varied from 9.93 to 10.62, to be compared with the best available elastic solution [3] 10.61. Thus the minicomputer solution 18 was in error by 6%, the other solutions by less than 4%.

The dimensionless load point compliance u_A EB/P varied from 48.1 to 55.11. To some extent the deflection depends on the local mesh refinement at the loading points as will be discussed below. The dimensionless crack mouth opening $2v_B$ EB/P varied from 29.2 to 32.42, to be compared with the best available elastic solution [3] 32.46.

4.2 Elastic-plastic solutions

Fifteen solutions could be pursued up to at least the specified 1.5mm deflection. Solution 5 stopped at 1.27mm, solution 15 at 1.31mm and solution 16 at 1.1mm. The two first accounted for finite geometry changes. In solution 16, no equilibrium iterations were used. The main results at the maximum deflection are summarized in Table 5. In solution 7 something went wrong. This solution shows that (human) errors are possible in this kind of problems, it will be plotted with the other solutions but it will not be taken into consideration in the discussion of the scatter of the results. Fig. 3 shows the load point displacement versus load curves. The scatter is roughly similar to that appearing in the ASTM round robin [2]. At the maximum deflection u_A= 1.27mm reached in the latter, the applied loads ranged from 30.7 to 42.8 kN. The present curves give for the same deflection loads ranging from 32.5 to 47.0 kN. The

TABLE 2 cont.ed (footnotes)

stiffest solutions are those using constant strain triangles (Nos. 1-3, 18). Solution 8 presents a stronger bend in the curve, probably due to using a two-slope stress-strain curve.

Fig. 4 represents the crack mouth opening displacement as a function of the applied load. The different solutions appear in the same order as in Fig. 3 and show a scatter which is comparable. Curves 6, 14 and 17 were so close one to the other that they were plotted as one curve; the same procedure was applied in some other figures. In Fig. 5 $\bar{J}$ is plotted as a function of the applied load. The relative positions of the curves are practically the same as in Fig. 3. In Fig. 6 which shows $\bar{J}$ versus the load point deflection the solutions appear in nearly the reversed order ($\bar{J}$ values of solution 7 should be multiplied by 2 to be consistent with Fig. 3). The scatter of the results is slightly larger than that obtained in the ASTM round robin [2]. Except in solution 11, the same paths as in the elastic analysis were used for calculating $\bar{J}$. The variation of J between the different paths was much larger than in the elastic case as shown in Table 5. As in the elastic case, a few participants applied in addition some forms of the virtual crack extension method which they generally considered to give better results than the path integral calculation.

Fig. 7 shows the calculated crack profiles along the first 10% of the crack length starting from the crack tip at the maximum specimen deflection u_A = 1.5mm. The relative distance d = 10% corresponds to a real distance of 1.27mm which is smaller than the crack tip element size used in some of the solutions. Various procedures were used for plotting the curves: joining the available displacement points by straight lines, using the displacement field of the crack

tip element, applying the HRR solution [4,5] fitted to the node adjacent to the crack tip, etc. It is evident from Fig. 7 that the prediction of the local deformation at the crack tip is very dependent on the mesh and assumptions used. Most of the reported profiles do not intersect the 45° line for which v = -x since in the immediate vicinity of the crack tip most FE models behave much too stiffly. For these reasons, six participants did not report any CTOD values. However, Fig. 7 shows that beyond d = 0.05 the scatter of the curves is much smaller than in the immediate vicinity of the crack tip and that a straight line extrapolation to x = 0 gives reproducible results for the half CTOD.

The 12 calculated CTOD versus u_A curves are plotted in Fig. 8. In eight cases the linear extrapolation procedure was applied, either to x = 0 or to the 45° line (which gave practically the same result). The straight line was drawn through two or more points (in the latter case using linear regression) on the v versus d plot; d values of these points varied from 0.09 to 1. Indeed, the whole crack flank is straight from d = 0.05 to d = 1. In three solutions (6, 9 and 15) the specified procedure was applied. One solution (No. 12) calculated the intersection of the 45° line with a curve representing the HRR displacement field fitted between the crack tip and the first node. The calculated CTOD curves in Fig. 8 do not show a larger scatter than the deflection curves in Fig. 3. However, there is a large scatter also in the elastic regime. Normally the CTOD versus u_A curves should be straight lines above, say, u_A = 0.25mm. This is not the case for solutions 5, 6, 9, 13 and 15. Deviations from the linear relationship could be interpreted as revealing inconsistencies in the analysis. Solutions 5 and 15 eventually stopped before reaching the required

maximum deflection. On the other hand the specified procedure for determining CTOD is possibly not a consistent one and might explain the deviations in solutions 6, 9 and 15. The ratio $\bar{J}$/CTOD at maximum deflection is given in the last column of Table 5. This ratio does not show any better constancy than $\bar{J}$ or CTOD themselves. The average $\bar{J}$/CTOD ratio is about 1010 MPa. Assuming that for a stationary crack it should be equal to 1.6 σ_y, this corresponds to an effective yield stress of 630 MPa.

The curves representing J_u calculated from Eq. (2) are not reproduced here. The curves showing e.g. J_u versus P are very similar to the $\bar{J}$ versus P curves plotted in Fig. 5. As can be seen from Table 5, the J_u values at the maximum deflection are in most solutions larger than the $\bar{J}$ values. However, considering the 15 solutions which exist up to u_A = 1.5mm, the difference between J_u and $\bar{J}$ is small compared with the overall scatter of the $\bar{J}$ results, except in solution 13 where this difference is 28% of $\bar{J}$.

5. DISCUSSION

This round robin reflects the variety of codes available and the freedom that their users have in choosing the manner that they think to be correct in running these codes for solving a numerical EPFM problem. Most participants knew reference [2], but declared that they had in no way modified their results after a comparison with it. Thus we can consider that the present round robin was not influenced by the prior publication of [2].

One of the 18 elastic-plastic analysis was wrong. The reviewer took the position to report it with the others but to ignore it in the evaluation of the state of the art of EPFM computer codes. The larger the number of solutions, the higher the probability that some of them contain human errors. This shows that for EPFM calculations needed for safety assessment, it is necessary to allocate sufficient manpower and time providing the possibility for careful checks preferably by independent analysis.

All 18 solutions of this round robin are correct within a few percent in the elastic regime. However, large differences appear in the elastic-plastic regime, increasing with increasing plastic deformation. The scatter of the results is of the same order or slightly larger than in [2] which included ten solutions. Of course a much larger number of participants should normally lead to a larger scatter. On the other hand one of the present solutions was obtained with remarkably modest means (a minicomputer). Even so, one has to state that no significant progress has been made in four years time in the state of the

art of numerical EPFM analysis.

Looking at the deformation-load behaviour in Figs. 3 and 4, one can distinguish three groups of results:

a) the four stiffest solutions 1, 2, 3 and 18 which used constant strain triangles;

b) the three softest solutions 5, 15 and 16 which stopped before the prescribed maximum displacement of 1.5mm;

c) the other solutions using 4-node or 8-node quadrilaterals.

The eleven solutions (c) are within a much more reduced scatter band. One is therefore tempted to look whether solutions (a) and (b) contained some features which could be considered as not recommendable. The premature stop of solution 16 may be due to not imposing equilibrium iterations which certainly should be done. Solutions 5 and 15 used large strain/displacement analysis which seems to lead easily to trouble with numerical convergence. However, two complementary results are interesting in this respect. The author of solution 6 based on small strain analysis also contributed an additional large strain analysis using the updated Lagrangian method. In this analysis he started from a finite crack tip radius of 0.03mm and obtained practically the same results as with the infinitesimal analysis reported in this paper. CTOD was obtained by subtracting 0.06mm from the CTOD given by the model. Very large strains (up to 400 per cent) appeared in the elements bordering the crack tip. Also the author of solution 17 reported he had performed an additional large strain analysis up to u_A = 1.5mm using the updated Lagrangian option in ADINA and obtained

practically the same results as with the small strain analysis. Anyhow, the development of reliable methods for large strain/ displacement analysis is a field in which much work is needed.

One of the four participants who used constant strain triangles claimed that the stiffer behaviour of the solutions listed as (a) above was due to the fact that the particular definition of load point displacement adopted in this round robin included the local deformations at the concentrated loads. He argued that for roughly the same element sizes in the neighbourhood of the point loads the 8-node quadrilateral solutions will show a larger penetration depth than the constant strain triangle solutions. This explanation of the stiffer behaviour of the constant strain elements is not satisfactory as can be seen from the following considerations. First, the influence of the local penetration under the concentrated loads vanishes in the crack mouth opening versus load curves and nevertheless Fig. 4 shows the same scatter as Fig. 3. The same holds for the $\bar{J}$ versus load curves of Fig. 5. Second, participant 13 made an additional analysis in which he eliminated the local deformations from the load point deflection by introducing for the latter $u_D - u_B$ instead of $u_A - u_C = u_A$. Curves 13 in Figs. 4 and 5 remained unaffected (they were only slightly prolongated since a somewhat larger load was required to produce the prescribed maximum load point deflection of 1.5mm). Curves 13 in Figs. 3 and 6 which contain u_A as one of the coordinates shifted to different positions. In Fig. 3 the change was small, the position of curve 13 fell close to 6/12/17. In Fig. 6 the change was larger, the new curve falling close to 6/11/17. The following numerical results were obtained at maximum deflection $u_D - u_B = 1.5$mm (in parenthesis the corresponding

values of the original solution 13 at $u_A = 1.5$mm):

P	= 36.9 kN	(35.9 kN)
$2v_B$	= 1.044mm	(0.867mm)
CTOD	= 0.305mm	(0.250mm)
J_u	= 285N/mm	(264N/mm)
$\bar{J}$	= 260N/mm	(206N/mm)
$J_u/\bar{J}$	= 1.10	(1.28)

One can observe that the original solution 13 probably presented the largest penetration depth at the concentrated loads amongst all the solutions. This is so because (a) solution 13 shows the largest change of position between the diagrams affected by (Fig. 3 and especially Fig. 6) and those unaffected (Figs. 4 and 5) by the local penetration, (b) as stated at the end of paragraph 4 the ratio $J_u/\bar{J}$ which should increase with increasing penetration depth was largest for this solution and (c), solution 13 was the only one in which the mesh was locally refined at both concentrated loads, points A and C in Fig. 1. Solution 1 in which the mesh was locally refined at point C seems also to include a large local deformation: curve 1 in Fig. 6 should normally be just below curve 18 in correspondence with the positions of curves 1 in Figs. 4 and 5.

We can conclude from this discussion that though the local deformations at the concentrated loads are responsible for some discrepancies between the order of the curves in the different plots, they do not essentially explain the scatter of the results. On the other hand, they are not responsible for the stiffer behaviour of the constant strain triangle solutions. Whether these solutions are too stiff or the other

solutions too soft is a question which can be answered only after the performance of experimental comparisons.

However, the interaction between the plastic zone at the load at point C and the crack tip plastic zone may be partly responsible for the scatter. Indeed, this difficulty would not be present in a problem in which the crack tip singularity is remote from any other singularities. This interaction was known right from the beginning to be the major drawback of the chosen three-point bend geometry since it is impossible to evaluate quantitatively. The advantage of being able to compare the results with the former ASTM round robin was however considered to be interesting enough to justify the repetition of the same problem.

CONCLUDING REMARKS

A meeting was held at the end of this round robin at which most contributors took part. Some of them expressed their belief that differences in the finite element meshes are more important than differences in the codes, in conformity with the results of a Japanese round robin [6]. The results of the present round robin are however in contradiction with this conclusion. As shown above, the results fall in three categories which are all dependent on the type of finite elements or the type of analysis used. No correlation between the dicretization and the scatter of the results can be found.

Those who had used 8-node isoparametric quadrilaterals considered them to be well suited to fracture problems due to the ease with which they can be collapsed to triangles at the crack tip and the possibility to allow a finite crack tip opening by using independent node numbers at the nodes of the elements converging at the crack tip. In that case mid-side nodes are to be preferred in order to avoid some of the difficulties asscciated with 1/4 point side nodes [7].

The determination of CTOD by linear extrapolation from remote crack side nodes is a convenient and reliable procedure, however it works only for edge cracks.

There is a strong interest in a continuation of numerical round robin activities. Comparisons with experimental results should be included in the next steps in order to draw conclusions on the relative merits of different numerical procedures. In view of the

large scatter of the elastic-plastic results, it is indeed a necessity to make efforts towards an improvement of the reliability of such analysis.

ACKNOWLEDGMENTS

Dr. J.D. HARRISON, Welding Institute, U.K., has given an appreciable help for the definition and start of this round robin. Mr. BLANCKENBURG has contributed in plotting the results. The author expresses his thanks to all participants who by spending a considerable time on this round robin, have made it a success.

REFERENCES

1 J.R. Rice, " A Path Independent Integral and the Approximate Analysis of Strain Concentration by Notches and Cracks ", Journal of Appl. Mech. , 35 (1968), pp. 379-386.

2 W.K. Wilson and J.R. Osias, " A Comparison of Finite Element Solutions for an Elastic-Plastic Crack Problem ", Int. Journal of Fracture, 14 (1978), pp. R95-R108.

3 H. Tada, P. Paris, G. Irwin, " The Stress Analysis of Cracks Handbook ", DEL Research Corp., Hellertown, USA (1973).

4 J.W. Hutchinson, " Singular Behaviour at the End of a Tensile Crack in a Hardening Material ", J. Mech. Phys. Solids, 16 (1968), pp. 13-31.

5 J.R. Rice and G.F. Rosengren, " Plane Strain Deformation Near a Crack Tip in a Power-Law Hardening Material ", J. Mech. Phys. Solids, 16 (1968), pp. 1-12.

6 M. Shiratori and T. Miyoshi, " A Comparison of Finite Element Solutions for J-integral Analysis of Compact Specimen (A Round Robin Test in Japan) ", in: Numerical Methods in Fracture Mechanics, D.R.J. Owen and A.R. Luxmoore, editors. Pineridge Press, Swansea, U.K., (1980), pp. 417-431.

7 L. Lamain, " On the Accuracy of EPFM Calculations ", 6th Int. Conference on Structural Mechanics in Reactor Technology, Paris, August 1981, Paper M 1/6.

TABLE 1 Participants in the EPFM Round Robin

Sv. Ib. ANDERSEN, O. GUNNESKOV	Risø National Laboratory	Denmark
H. ANDERSSON, E. LARSSON	National Testing Institute Borås	Sweden
M.A. ASTIZ, M. ELICES	Madrid Technical University	Spain
A. BAKKER	Delft University of Technology	Holland
S. BHANDARI	Novatome	France
A. CELLA	CISE	Italy
J.L. CHEISSOUX, P. CHOUARD	CEA Cadarache	France
L. GRUETER, R. RÜTTENAUER	Interatom	F.R.Germany
G.T.M. JANSSEN	T.N.O. Institute for Mechanical Constructions	Holland
A.P. KFOURI, K. MILLER	University of Sheffield	U.K.
L. LAMAIN	JRC Ispra Establishment	C.E.C.
P. LEMOINE	CEA Saclay	France
A. LUXMOORE, M.H. BLEACKLEY	University of Wales, Swansea	U.K.
K. MARKSTRÖM	Royal Institute of Technology	Sweden
G. OERTLI	Sulzer Brothers	Switzerland
C. de PATER, R.M.E.J. SPIERING	Twente University of Technology	Holland
W. SCHMITT	Fraunhofer-Institut für Werkstoffmechanik	F.R. Germany
C.E. TURNER	Imperial College of Science and Technology	U.K.

TABLE 2

Finite Element Codes and Numerical Methods

Ref.	Code	Numerical method	Equilibrium iteration within each load increment	No.of loading steps	Stress-strain curve
1	Own	Initial stress	Yes	24	As specified
2	Own	Tangent modulus	No (3)	45	4 linear segments (14)
3	Own	Tangent modulus	(4)	160	(15)
4	Own	Tangent modulus	Yes (5)	20	11 linear segments
5	Own (1)	Initial stress	Yes (6)	28	(16)
6	Own	Tangent modulus	No (3)	44	As specified
7	NONSAP	Tangent modulus		27	
8	NONSAP	Tangent modulus	Yes (7)	21	Bi-linear (17)
9	MARC	Tangent modulus	Yes (8)	40	As specified
10	Own	Initial stress	Yes (9)	564	149 linear segments
11	Own	Initial stress	Yes (10)	15	22 points (18)
12	Same as 11	Initial stress	Yes (10)	15	5 points (18)
13	Own	Tangent modulus	No	25	As specified
14	Own	Tangent modulus	Yes (11)	60	As specified
15	ADINA (1)	Tangent modulus	Yes	21	As specified
16	ADINA	Tangent modulus	No	12	As specified
17	ADINA	Tangent modulus	Yes (12)	15	Multi-linear
18	Own (2)	Tangent modulus	Yes (13)	113	As specified

TABLE 2 cont.ed (footnotes)

/1/ Large strain/displacement analysis.

/2/ Implemented on a PDP 11-34 minicomputer.

/3/ A corrective load vector is calculated and added to the next load increment.

/4/ Gauss-Seidel iteration. Absolute sum of nodal displacement increments 10^{-7} times absolute sum of nodal displacements.

/5/ Newton-Raphson, force equilibrium criterion $\Delta F/F \leq 0.005$.

/6/ Equilibrium and yield criterion satisfied anternately. Criterion for convergence: equivalent stress at sensor points $<$ A times current yield stress, A typically 1.005 to 1.015.

/7/ Norm of incremental displacements < 0.001 times the norm of total displacements.

/8/ Difference between estimated and calculated energy change during a load step $<$ 5 per cent.

/9/ Modified Newton-Raphson. Criterion for convergence: norm of residual forces $\leq$ 6 per cent of norm of total external forces.

/10/ Two iteration levels. Internal iterations in which stresses are iterated back to the uniaxial stress-strain curve. External iterations solving explicitely the equilibrium equations using the inversed stiffness matrix. Iterations stop when equivalent stresses in all elements at two successive iterations coincide within one per cent. Explicit integration of Prandtl-Reuss equations.

/11/ Newton-Raphson. Criterion for convergence: norm of residual force vector less than 25 N. Subintegration procedure: normal to the flow surface is calculated 9 times per load step to evaluate the stress.

/12/ Both load balance and displacement convergence checks were performed using standard ADINA tolerances.

/13/ Gauss-Seidel iteration. Sum of absolute differences between displacements in two iterations less than specified value, corresponding to three significant digits in stress values.

/14/ Four-fraction Besseling hardening model.

/15/ As specified except that a line was drawn from yield to be tangent to the power law to avoid the actual discontinuity.

/16/ As specified except $E = 2.177 \times 10^5$ MPa, $\sigma_y = 380$ MPa.

/17/ $\sigma_y = 500$ MPa, $E_t = 2800$ MPa.

/18/ Parabolic interpolation.

TABLE 3 Finite Element Models

Ref.	DOF	Elements	Nodes	Finite element (far field)	Crack tip elements	
					Type	Size, mm
1	557	508	288	Constant strain triangles	Normal	0,35
2	566	521	294	Constant strain triangles	Normal	0,095
3		781	435	Constant strain triangles	Normal	0,08
4	952	419	476	4-node quadrilaterals, 4 integration points	Normal	0,635
5	557	252	285	4-node isoparametric quadrilaterals, sensors located at nodes	Normal	0,13
6	389	168		4-node isoparametric quadrilaterals	Quadrilaterals collapsed into triangles	0,4
7	514	85		8-node isoparametric quadrilaterals, 2x2 integration points, either rectangular or collapsed into triangles	Normal (rectangular)	0.51
8	708	108	363	8-node isoparametric quadrilaterals, 3x3 integration points	Normal	0.5
9	471	68	243	8-node isoparametric quadrilaterals, 3x3 integration points	Quadrilaterals collapsed into triangles, 1/4 point side nodes, independent tip nodes	0.635
10	378	54	189	8-node isoparametric quadrilaterals, 2x2 integration points	Normal	2.2
11	766	116	383	8-node isoparametric quadrilaterals, 3x3 Gauss points, 6-node triangles with 7 Hammer points	Normal quadrilaterals	0.32

TABLE 3 cont.ed Finite Element Models

Ref.	DOF	Elements	Nodes	Finite element (far field)	Crack tip elements Type	Size, mm
12	834	144	429	Same as 11	Normal triangles	0,25
13	524	87	262	8-node isoparametric quadrilaterals, 2x2 integration points, 6-node isoparametric triangles with cubic 4 point integration scheme	Normal triangles	0.4
14	454	69	234	8-node isoparametric quadrilaterals, 3x3 integration points	Quadrilaterals collapsed into triangles, 1/4 point side nodes, one DOF at crack tip	1,3
15	687	102	351	8-node isoparametric quadrilaterals, 3x3 integration points	Quadrilaterals collapsed into triangles, 1/4 point side nodes, independent tip nodes	2,1
16	506	75	264	8-node isoparametric quadrilaterals, 2x2 integration points	Quadrilaterals with 3x3 integration points collapsed into triangles, 1/4 point side nodes, independent tip nodes	0.635
17	395	56	203	8-node isoparametric quadrilaterals, 2x2 integration points	Quadrilaterals collapsed into triangles, mid point side nodes, indep. tip nodes	1,3
18	236	191	118	Constant strain triangles	Normal	0,5

TABLE 4 ELASTIC CALCULATIONS

REF.	Non-dimensional results			J calculations				
	K_1	u_A	v_B	Number of paths	Mean radius(mm) Min	Max	$(J/\bar{J})$min	$(J/\bar{J})$max
1	10.23	50.78	30.68	10	0.7	5.3	0.969	1.042
2	10.2	49.8	30.4	2	0.347	0.435	0.999	1.001
3	10.38	49.91	31.19	6	0.62	11.5	0.993	1.019
4	10.27	52.05	31.21	5	4.3	10.75	0.992	1.009
5	10.28	49.02	30.69	4	0.18	11.4	0.973	1.027
6	10.45	52.6	31.7	8	0.7	14.1	0.991	1.017
7	10.43	54.53	31.98	4	0.97	14.6	0.972	1.033
8	10.34	53.62	32.03	5	2.25	13.0	0.978	1.010
9	10.31	52.15	32.26	5	0.635	8.00	0.977	1.021
10	10.19	52.41	31.55	4	6.8	13.1	0.978	1.047
11	10.53	53.93	32.15	3	5.73	10.7	0.993	1.007
12	10.56	53.86	32.21	7	0.56	10.4	0.990	1.015
13	10.47	55.11	31.96	6	0.96	5.68	0.997	1.003
14	10.59	53.94	32.39	10[a]	1.35	11.1	0.975	1.052
15	10.62	53.96	32.32	6	3.58	10.9	0.995	1.003
16	10.49	55.10	32.25	6	1.6	19.3	0.986	1.008
17[b]	10.58	54.13	32.42	8	0.71	11.4	0.991	1.025
18	9.93	48.1	29.2	3	0.5	6	0.990	1.015

a) $\bar{J}$ was calculated as the average of the following 10 values: 6 paths through integration points, 2 paths through nodes, 2 virtual crack extension J values.

b) A separate model with quarter point singularity elements at the crack tip was set up for the elastic analysis.

TABLE 5 ELASTIC-PLASTIC CALCULATIONS

REF.	Values at u_A = 1.5 mm (except otherwise specified)							
	P (kN)	$2r_B$ (mm)	CTOD (mm)	J_u (N/mm)	$\bar{J}$ (N/mm)	$(J/\bar{J})$min	$(J/\bar{J})$max	$\bar{J}$/CTOD (MPa)
1	46.1	0.976	0.229	320	276	0.868	1.244	1205
2	42.5	1.04	0.287	305	330	0.996	1.004	1150
3	42.8	1.06		302	302	0.81	1.23	
4	41.5	1.02		342	314	0.936	1.057	
5[a]	32.7	0.874	0.217	209	172			793
6	37.2	1.04	0.283	277	265	0.980	1.038	936
7	58.0	0.938	0.201	200	194	0.911	1.087	965
8	39.0	1.03		293	288	0.906	1.05	
9	37.8	1.06	0.273	279	250	0.960	1.041	916
10	39.7	1.02		294	269	0.949	1.067	
11[b]	38.0	1.03	0.301	279	264	0.997	1.003	877
12	37.1	1.04	0.198	271	267	0.987	1.060	1350
13	35.9	0.867	0.250	264	206	0.891	1.054	824
14	36.8	1.02	0.291	273	237	0.822	1.073	814
15[c]	33.1	0.886	0.135	210	187	0.967	1.032	1385
16[d]	33.5	0.63		177	140			
17	37.0	1.04	0.290	272	262	0.970	1.013	903
18	49.4	0.989		334	346	0.889	1.130	

a) Calculated values are at u_A = 1.27mm

b) Only two paths were used for J calculation, mean radii 4.30 and 5.73mm

c) Calculated values are at u_A = 1.31mm

d) Calculated values are at u_A = 1.1mm

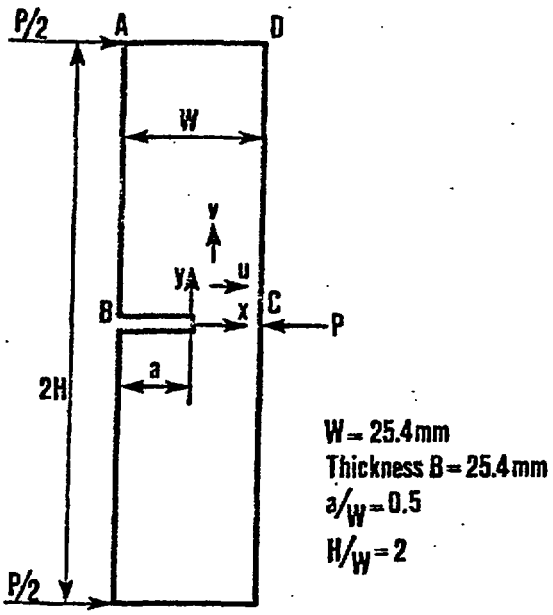

Fig. 1 - Three-point bend geometry and loading conditions

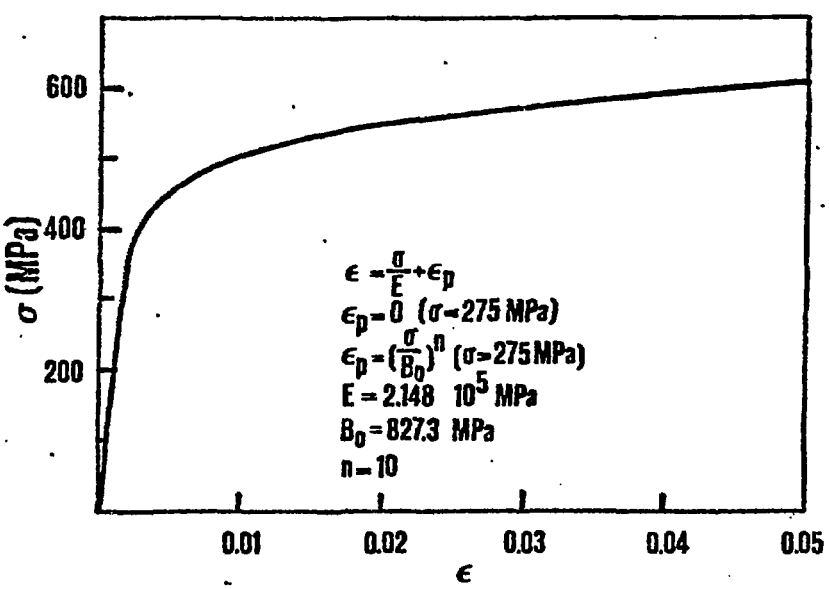

Fig. 2 - Uniaxial stress-strain curve

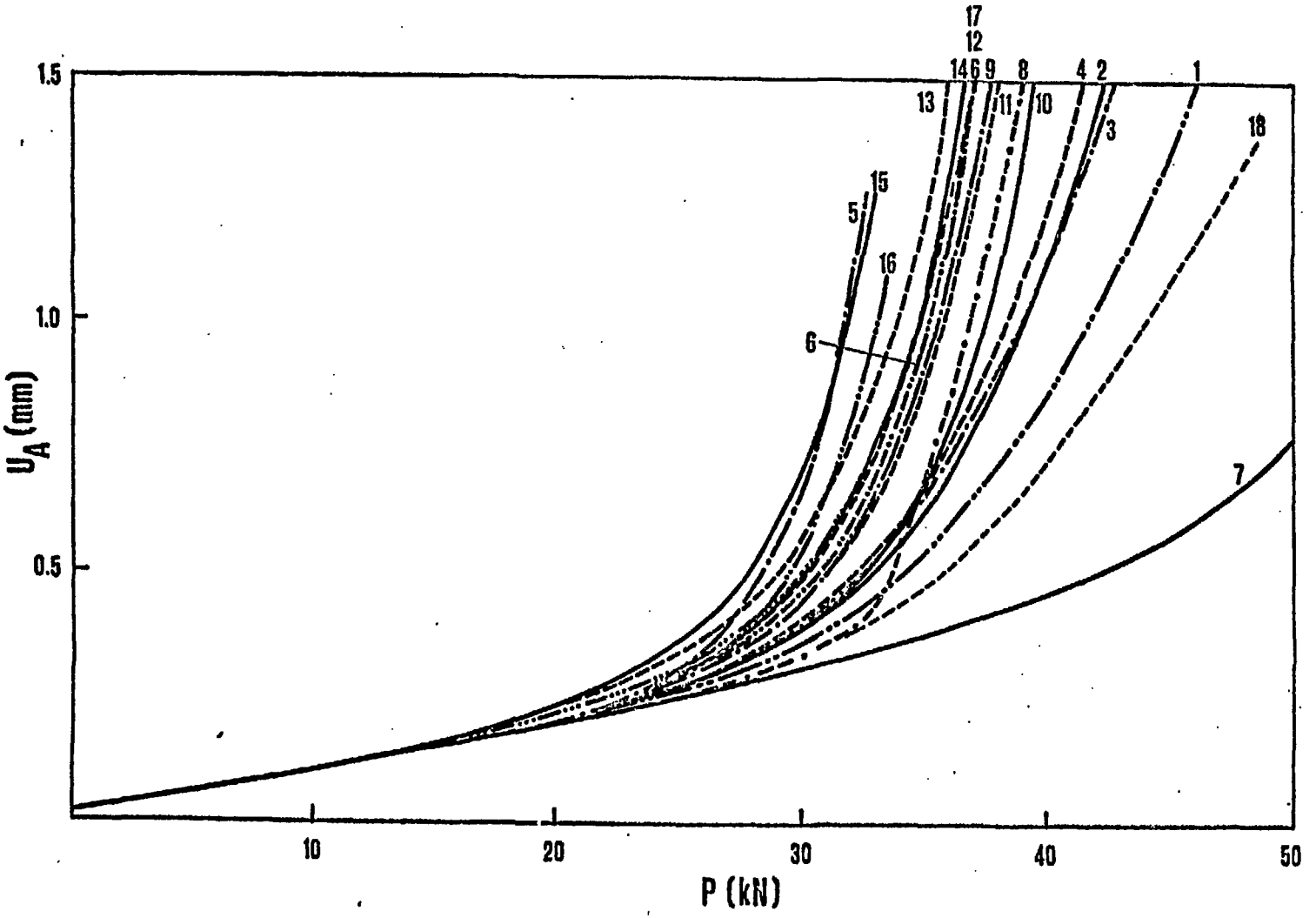

Fig. 3 - Load-displacement curves

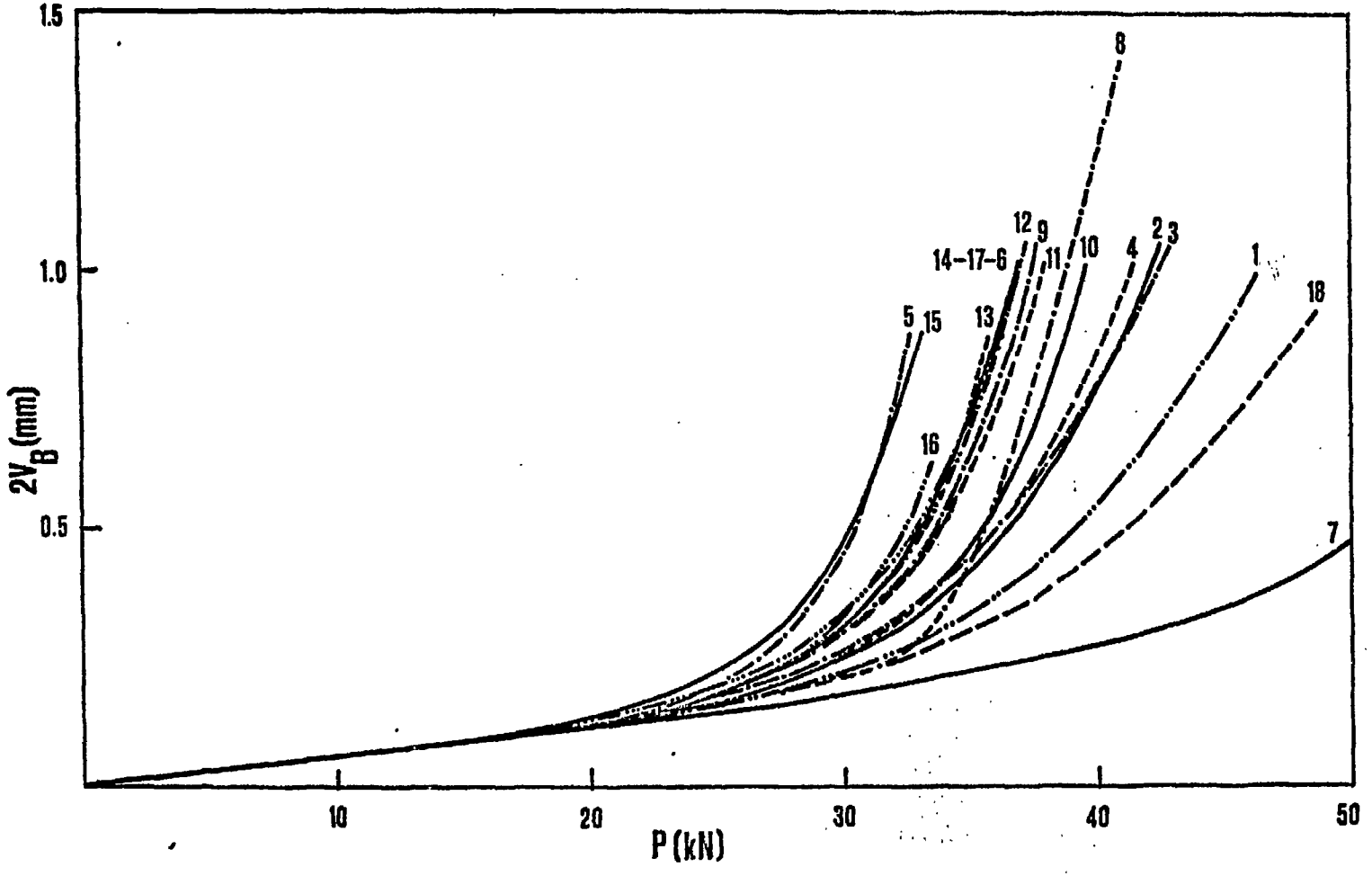

Fig. 4 - Crack mouth opening versus load

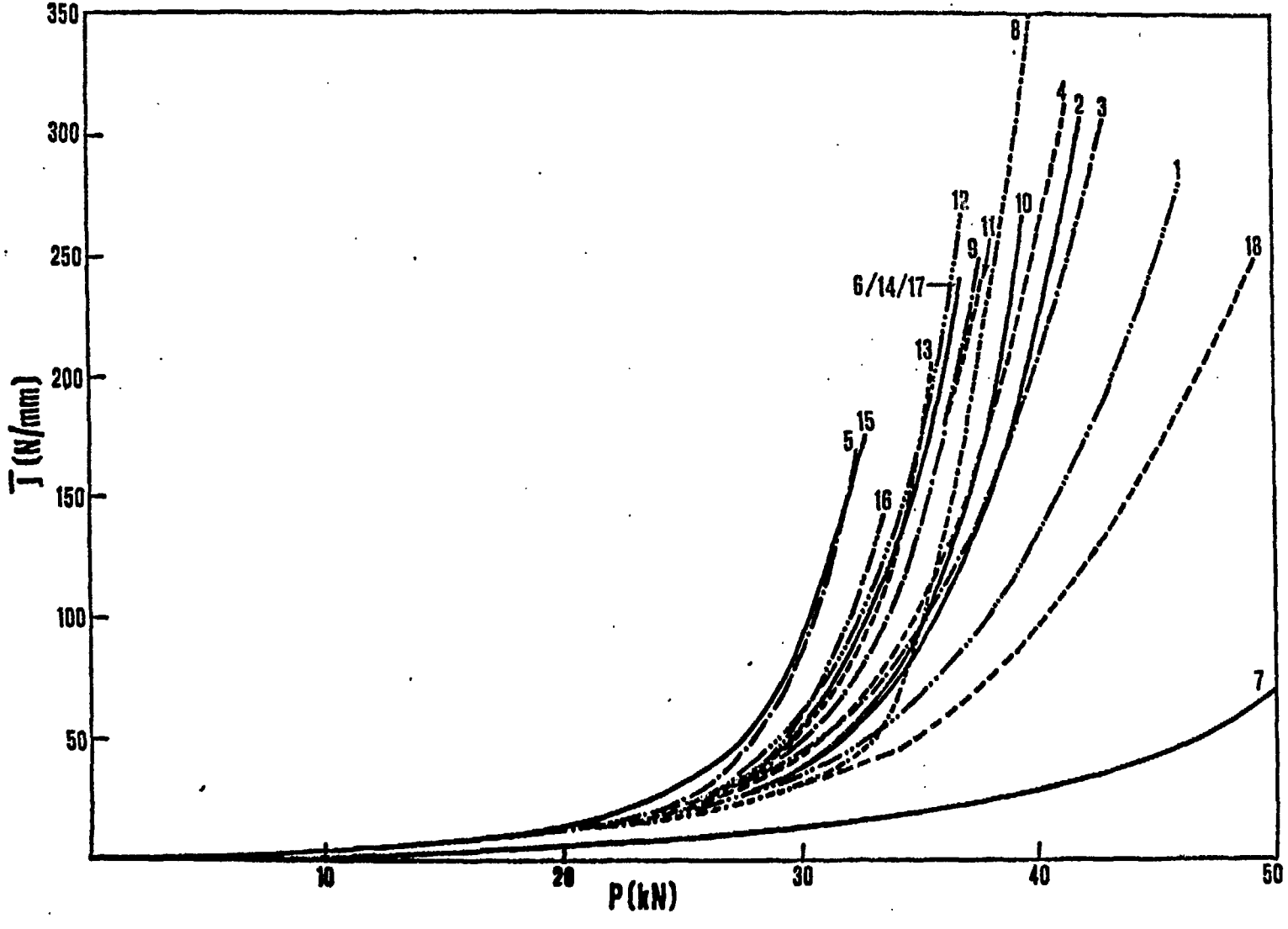

Fig. 5 - Path integral $\bar{J}$ versus load

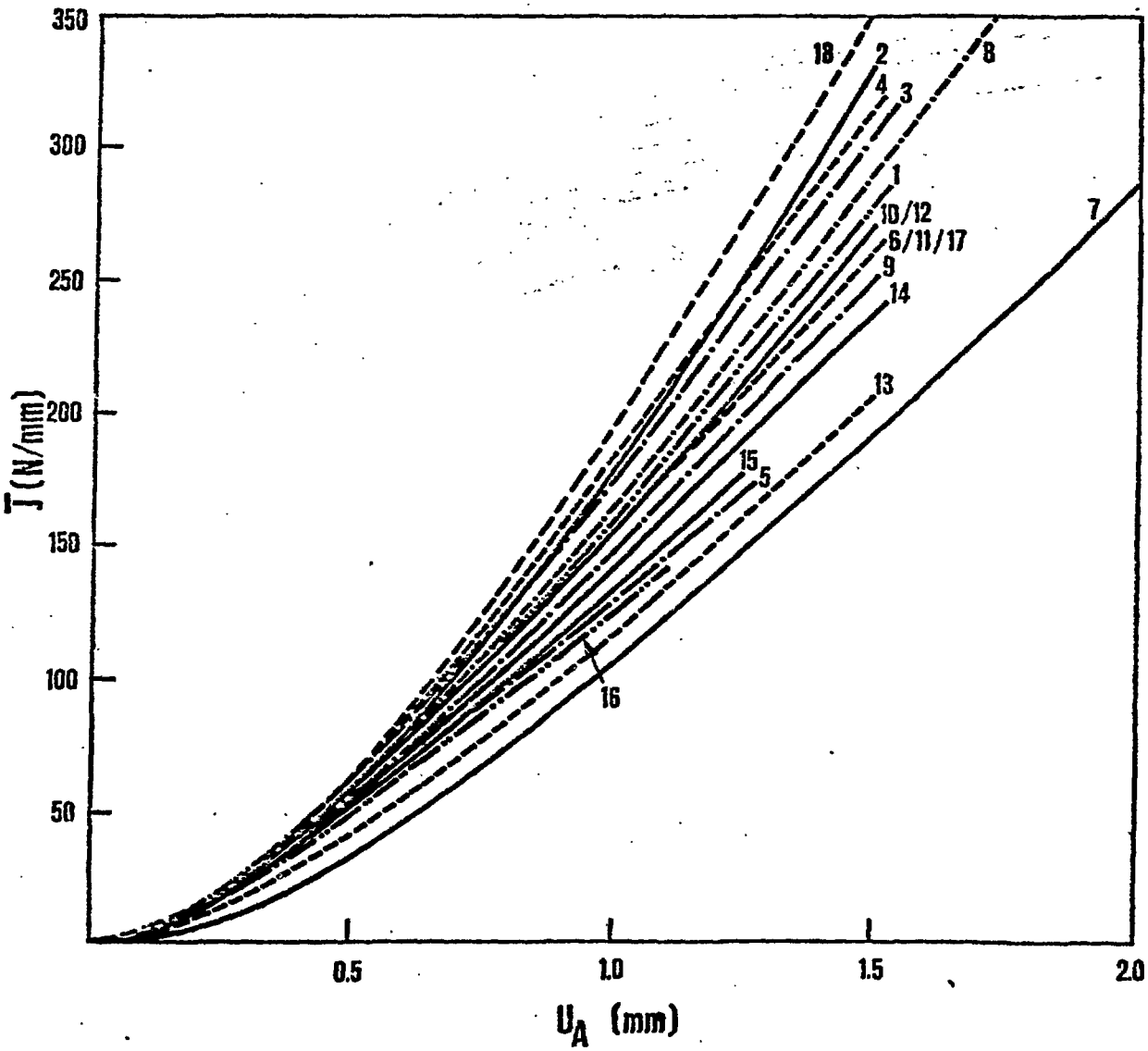

Fig. 6 - Path integral $\bar{J}$ versus load point displacement

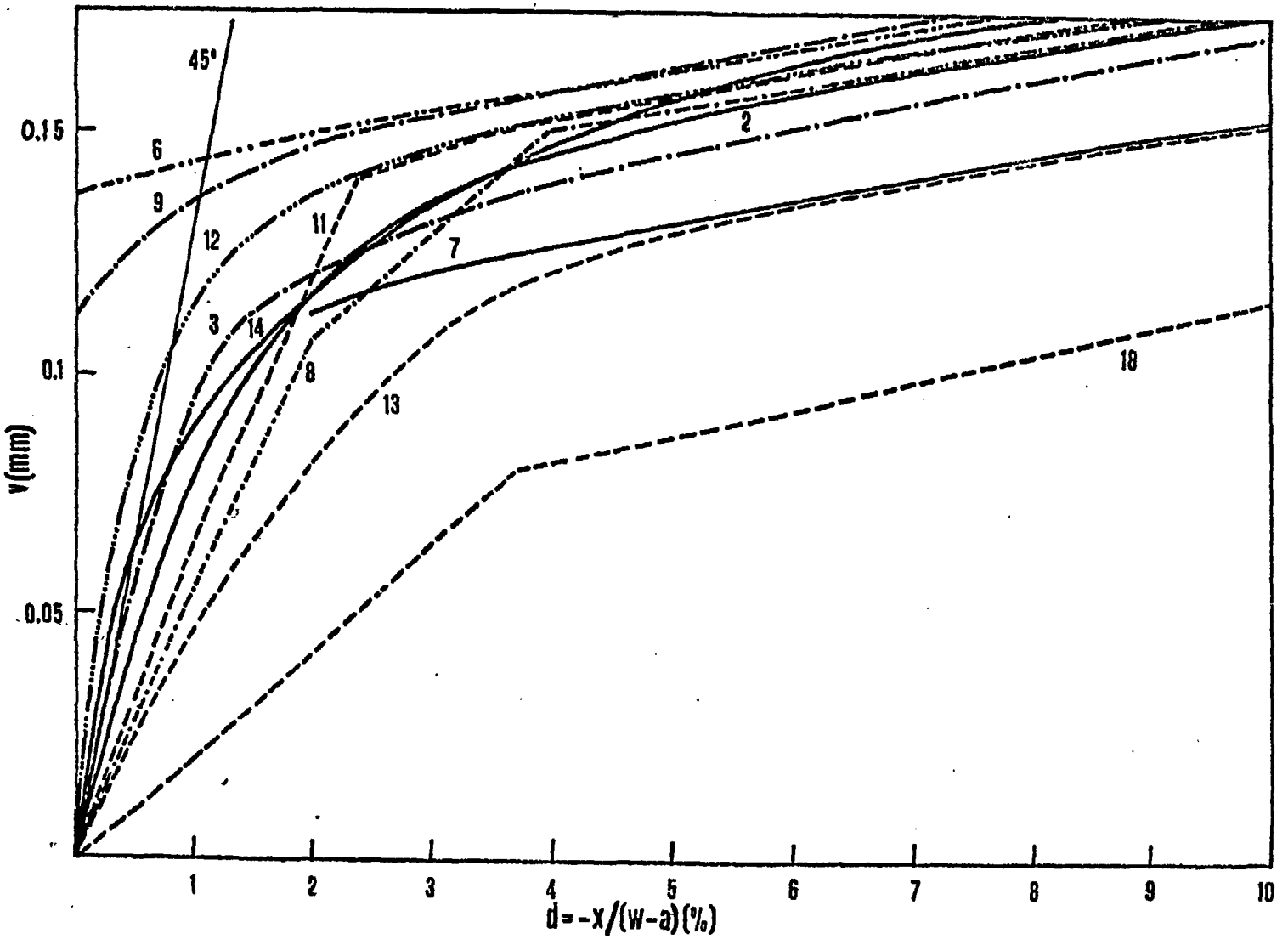

Fig. 7 - Crack tip profiles

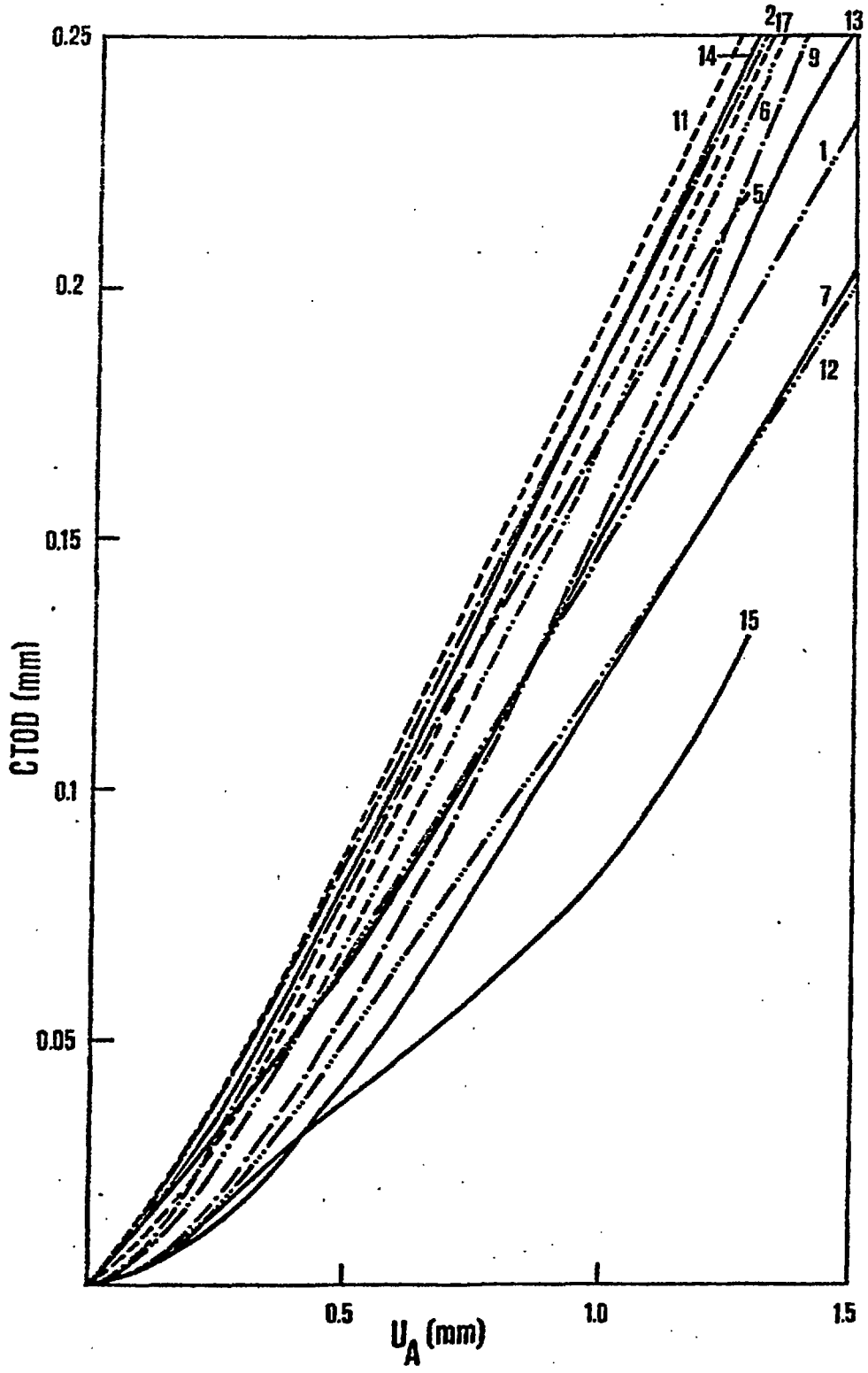

Fig. 8 - CTOD versus load point displacement